공학석사학위논문

Preparation of Highly Reinforced Pore-filling Electrolyte Membranes from Cross-linked Benzoxazine-Benzimidazole Copolymers for Fuel Cell Applications

가교된 벤족사진-벤즈이미다졸 공중합체를 이용한 강화된 다공 충진 막의 제조와 연료전지로의 응용

2013年 2月

서울대학교 대학원

화학생물공학부

김기현

Preparation of Highly Reinforced Pore-filling Electrolyte Membranes from Cross-linked Benzoxazine-Benzimidazole Copolymers for Fuel Cell Applications

가교된 벤족사진-벤즈이미다졸 공중합체를 이용한
강화된 다공 충진 막의 제조와
연료전지로의 응용

指導敎授 李 鍾 贊

이 論文을 工學碩士 學位論文으로 提出함

2013年 2月

서울大學校 大學院
化學生物工學部
金 機 炫

金 機 炫의 工學碩士 學位論文을 認准함

2012年 12月

委 員 長 _____ (印)

副委員長 _____ (印)

委 員 _____ (印)

Preparation of Highly Reinforced Pore-filling Electrolyte Membranes from Cross-linked Benzoxazine-Benzimidazole Copolymers for Fuel Cell Applications

by

Kihyun Kim

February 2013

Thesis Adviser: Jong-Chan Lee

[Abstract]

An ultrathin novel reinforced pore-filling polymer electrolyte membrane (20um, thick) based on sulfonated poly(arylene ether sulfone) (PAES60) impregnated porous substrate, was prepared by polymer filling method for using in proton exchange membrane fuel cells (PEMFCs) application. Cross-linked copolymer synthesized with poly[2,2'–(*m*–phenylene)–5,5'–bibenzimidazole] (PBI) and 3–phenyl–3,4–dihydro–6–*tert*–butyl–2H–1,3–benzoxazine (*p*Bu) was selected as a substrate (P(*p*Bu-co-BI)). Porous substrates were successfully fabricated by leaching out a low molecular weight compound using a selectively soluble solvent of the porogen from P(*p*Bu-co-BI) / porogen mixtures. The pore size and porosity of the substrate were determined by the P(*p*Bu-co-BI) / porogen ratio and confirmed by SEM, mercury intrusion method and density measurement method. Filling material, PAES60, was synthesized successfully via nucleophilic aromatic substitution polymerization. In comparison to a pristine PAES60 membrane, pore-filling membrane (PF-PAES60) showed extremely low dimensional change (4-13%), water uptake (10-18%), outstanding mechanical strength and increased chemically bounded water. However, the proton conductivity of PF-PAES60 was lower than that of pristine

PAES60 membrane. All of these results can be attributed to the reinforcement effect of porous P(*p*Bu-co-BI) substrate and acid-base interaction between imidazole groups in the substrate and sulfonic acid groups in the filling polymer.

Keywords: reinforced pore-filling polymer electrolyte membrane, proton exchange membrane fuel cells, PAES60, P(*p*Bu-co-BI), porogen , PF-PAES60

Student number: 2011-21013

TABLE OF CONTENTS

LIST OF FIGURES

LIST OF TABLES

LIST OF SCHEMES

1. INTRODUCTION

Among the different types of fuel cells, the polymer electrolyte membrane fuel cell (PEMFC) has the most promising future as a power source for car application [1]. But large-scale development of the PEMFC is still limited by the necessary improvement of some key components, especially the proton exchange membrane (PEM). Thin PEM with proper proton conductivity at high temperature is a key factor for applying electric transportation because of necessitating high power density [2]. For making the stabilized thin PEM, there are many studies on the strategies for improving the mechanical strength and dimensional stability, such as cross-linking [3, 4], blending [5], block copolymerization [6] and composite PEMs [7-10]. Especially, composite membranes consisting of polymer electrolyte matrices and organic/inorganic fillers have been studied significantly because of the controllable chemical and physical properties produced by combining different properties of components. “Pore-filling” is another concept to prepare composite membrane. Pore-filling membrane is composed of a proton conducting electrolyte and mechanically reinforcing porous substrates [11-15]. Particularly, in the reinforced pore-filling membranes, representative examples of porous substrates include poly(tetrafluoroethylene) (PTFE) [11, 12], polycarbonate [13], polyvinylidene fluoride (PVDF) [14] and polyimide [15], wherein

porous structure, compatibility with filling electrolytes, and physicochemcal stability of porous substrates are considered to be key factors significantly affecting the performances of pore-filling membranes.

In this study, we develop new reinforcing cross-linked structured porous substrates, which were comprised of polybenzoxazine (PBOA) and polybenzimidazole (PBI). In previous experiments, we already demonstrate the excellent physicochemical properties and performances of cross-linked PBOA and PBI copolymer P(BOA-co-BI) [16, 17]. For introduction of the porosity into the P(BOA-co-BI) membranes, dibutyl phthalate (DBP) was used as a porogen compound [18]. This method allows easily control the pore-size and porosity by changing the porogen content. P(BOA-co-BI) porous substrate exhibited strong mechanical properties, a well–developed porous structure and good water retention capability at low humidity condition owing to the acid-base interaction with the sulfonated filling material. Acid-base interaction served as a physicochemical support offering stability to the pore-filling membrane because of inducing the ionic cross-linking [19, 20]. This feature can make possible to using the high degree of sulfonation polymer as a filling material.

Sulfonated poly(arylene ether sulfone) (PAES) is selected as a proton conducting ionomer to be impregnated into the reinforcing porous substrate because of its high thermal stability, good chemical resistance and excellent mechanical strength. Above all, most advantage of PAES ionomer is easily obtained high proton conductivity by controlling the

degree of sulfonation. In this experiment, degree of sulfonation 60 PAES (PAES60) was selected as a filling material. In generally, high degree of sulfonation PAES tend to have low mechanical stability in water due to a high water uptake, large dimensional change [21]. Hence, the impregnation of PAES60 into P(BOA-co-BI) substrate is expected to be a most effective approach to overcome these shortcomings. Because our pore-filling membrane take advantage of not only reinforced effect from the substrate but also ionic cross-linking between the porous substrate and filling material.

The structure of the PAES60 pore-filling (PF-PAES60) membrane was characterized and confirmed by scanning electron microscopy (SEM) coupled with energy dispersive spectroscopy (EDS). In addition, the physicochemical and electrochemical properties of the membranes, e.g. mechanical property, water uptake, dimensional stability and proton conductivity, were investigated. TGA analysis was conducted to compare the state of water, i.e. physically adsorbed water and chemically adsorbed water, in membranes. For comparison of properties, pristine PAES60 membrane was also employed.

Additional interaction between the porous P(*p*Bu-co-BI) substrate and PAES60 was confirmed by the Fourier transform infrared (FT-IR) spectroscopy and mechanical strength measured by universal testing machine (UTM).

2. EXPERIMENTAL

Materials.

4,4'-Diclorodiphenyl sulfone (DCDPS, 99% Aldrich) and 4,4'-dihydroxybiphenyl (BP, 99% Aldrich) were recrystallized from toluene and methanol respectively. 3,3'-Disulfonated-4,4'-diclorodiphenyl sulfone monomer (SDCDPS) was synthesized from DCDPS and fuming sulfuric acid (65% SO_3, Merck) according to previous report [22]. SDCDPS was purified by recrystallization in distilled water and iso-propanol mixture. Toluene (99.5%, Junsei) was refluxed over calcium hydride and distilled. *N*-Methyl-2-pyrrolidone (NMP, 99.0%, Junsei) was stored over molecular sieves under nitrogen. Potassium carbonate (K_2CO_3, 99.0+%, Aldrich) was dried under vacuum prior to use. Isophthalic acid (99%, Aldrich) was purified by recrystallization in ethanol to obtain white needle–like cystals. 3,3'–diaminobenzidine (97%, Tokyo Kasei, TCI), polyphosphoric acid (PPA, 116% H_3PO_4, Junsei), and phosphorous pentoxide (97%, Aldrich). 4–*tert*–Butylphenol (99%), *p*–formaldehyde (95%), aniline (99%) and Dibutyl phthalate (DBP, 99%) were purchased from Aldrich and used without further purification. Other solvents were used as received.

Synthesis and film preparation

[2.1.1 Synthesis of PAES60 and preparation of pristine PAES60 membrane]

The molar ratio of the SDCDPS monomer to DCDPS monomer determined degree of sulfonation. In this experiment, we synthesized PAES60, where 60 is the molar ratio of SDCDPS to DCDPS. Synthetic procedure of PAES60 conducted according to following procedure. 5.00 g (26.9 mmol) of DHBP, 3.09 g (10.8 mmol) of DCDPS, 7.93 g (16.1 mmol) of SDCDPS, 4.28 g (30.9 mmol) of K_2CO_3, 62.4 mL of NMP (~20 wt%), and 31.2 mL of toluene were charged into a three-neck flask equipped with nitrogen inlet, mechanical stirrer, condenser, and Dean-Stark trap. The reaction was heated at 150 ^{o}C for 4 h to ensure complete dehydration as an azeotrope with toluene. And then toluene was removed over a 1 h interval. The Dean-stark trap was emptied and the temperature was slowly increased to 190 ^{o}C for 24 h to obtain a viscous solution. After cooling to room temperature, 10.0 mL of NMP was added to dilute this solution. The homogeneous solution was filtered to remove the salt and decanted into *iso*-propylalcohol (1000 mL) to isolate the polymer. The fibrous precipitate was obtained

by filtration and rinsed with *iso*-propylalcohol. The resultant was then dried 24 h under vacuum at 60 ^{o}C, Yield: >90%.

Pristine PAES60 (10 wt. % in DMAc) membrane was prepared by solution casting method by using the doctor blade [23].

[2.1.2 Preparation of porous P(*p*Bu-co-BI)-X membranes]

Synthetic procedures of poly[2,2'-(m-phenylene)-5,5'-(bibenzimidazole)] (PBI) and 3-Phenyl-3,4-dihydro-6-tert-butyl-2H-1,3-benzoxazine (*p*Bu) were described in our previous report.

In this experiment, the selected weight% of *p*Bu to PBI was 100.

Porous P(*p*Bu-co-BI) films were fabricated by different wt % of Dibutyl phthalate (DBP, 99%) which is used as porogen-plastisizer by solution casting. The weight ratio of P(*p*Bu-co-BI) to DBP were represented by P(*p*Bu-co-BI)-X. X means the DBP content to P(*p*Bu-co-BI) weight percent.

The following procedure was used for the preparation of P(*p*Bu-co-BI)-90. Other films which contained different weight ratio of DBP were fabricated by same procedure. Solution containing 0.68 g of PBI powder, 0.68 g of *p*Bu and 1.22 g of DBP was cast onto clean flat glass plate by using solution casting method. Doctor blade was used to control the thickness of blended solutions. Thermal treatment of casted

membranes was conducted according to our previous method [16]. After thermal treatment, DBP was extracted by immersing the membranes in methanol for 1 h [18]. And then porous P(*p*Bu-co-BI)-90 washed with 80 ^{o}C deionized water three times to remove the residual solvents on the surface of the membrane. Finally, the resulting membrane was dried at room temperature under vacuum for 24 h.

[2.1.3 Preparation of PF-PAES60 membrane]

PF-PAES60 was fabricated by the polymer solution dipping method [14]. The Porous P(*p*Bu-co-BI)-90 substrate was immersed in PAES60 polymer solution (10 wt. % in DMF) for 2 h at 60 ^{o}C to fill the pores of the substrate. The PAES60 polymer impregnated membrane was unfolded on the glass plate and dried at 80 ^{o}C. The dipping and drying process were repeated three times in order to ensure complete impregnation of PAES60 solution into the pores of the porous P(*p*Bu-co-BI)-90 substrate. After these circumstances, PAES60 pore-filling membrane (PF-PAES60) was vacuum dried at 120 ^{o}C for 24 h to remove the residual solvent perfectly. Then cooling to room temperature, the pore-filling membrane was soaked in distilled water and peeled off the glass plate. The obtained membrane was dried using gel dryer at 60 ^{o}C for 1 h, and then the film was located to a vacuum

oven for additional drying for 12 h.

[2.1.4 Protonation of pristine X membrane and PF-X membrane (Na^+ to H^+)]

The membranes in sodium salt form were transformed to their acid form by soaking in 1 M H_2SO_4 aqueous solution at room temperature for 24 h. After that, the membranes (in acid form) were rinsed with distilled water several times and then dried using gel dryer at 60 ^oC for 1 h. Finally the membranes were located to a vacuum oven for additional drying for 12 h.

Analysis

[2.2.1 Morphological analysis and SEM, EDS measurements]

Average pore diameters and porosity of the porous P(*p*Bu-co-BI)-X substrates generated by different weight ratio of DBP content were measured by mercury porosimetry using a MICROMERITICS AUTOPORE Ⅳ 9500 instrument. Density of the substrates was calculated by using a flotation weight loss method in a 4-decimals-precision Gram Precision balance [18].

The porosity of the substrates (ϕ_p) was also estimated using the

following relationship equation [25]

$$\oint p = \left\{1 - \frac{w_{sub}}{\rho_{sub} * V_{sub}}\right\} \times 100 \quad (1)$$

Where w_{sub}, ρ_{sub} and V_{sub} are the weight, density and volume of the porous P(*p*Bu-co-BI) substrate, respectively.

The cross-sectional morphology of the porous P(*p*Bu-co-BI)-X substrates and PF-PAES60 membrane was characterized by field emission scanning electron microscope (FE-SEM, Carl Zesis, Germany) equipped with EDS. In PF-PAES60 membrane, the distribution of carbon, nitrogen, sulfur and sodium elements along the membrane cross-section was determined by an EDS mapping method [24]. To confirm the distribution of the sulfonic acid group of the PAES60 ionomer in the pore-filling membrane, PF-PAES60 (in H^+ form) was reconverted to the Na^+ form by immersing it in 1M NaOH solution for 24 h. From this process, the sodium (Na) element was used as a signal of the -SO_3H group in neutralized PAES60 ionomer.

[2.2.2 Characterization]

The ^{1}H NMR analyses conducted on a Brucker Avance 500 with a proton frequency of 500 MHz. Spectra were collected from an PAES60 solution in deuterated dimethyl sulfoxide (DMSO-d_6) and tetramethylsilane (TMS) used as an internal standard. Ion Exchange Capacity (IEC) values of PAES60 was determined by ^{1}H-NMR spectra [23] and titration with 0.01 M aqueous NaOH solution. Gel permeation chromatography (GPC) measurement of PAES60 solution in DMF was conducted. A standard curve was created from a polystyrene standard solution (TSK, Tosoh Corp.).

The FT-IR spectra of porous substrate, pristine PAES60 membrane and PF-PAES60 membrane were measured in the attenuated total reflectance (ATR) mode in the frequency range of 4000-650 cm^{-1} on a Nicolet 6700 instrument (Thermo Scientific, USA). All spectra were recorded as the average of 32 scans with the resolution of 8 cm^{-1}.

The water uptake of the PAES60 and PF-PAES60 membranes determined after the sample membranes were immersed in Deionized water at defined temperature. Water uptake (ΔW) of the PAES60 and PF-PAES60 membranes was calculated using the following equation [26].

$$\Delta W\ (\%) = \frac{W_{mem}^{s} - W_{mem}^{d}}{W_{mem}^{d}} \quad (2)$$

Where W_{mem}^{s} is the weight of membranes in the swollen state at given temperature for 24 h. and W_{mem}^{d} is in the dry state.

Dimensional Change in membrane volume (ΔV) between the swollen state and the dry state of the PAES60 membrane and PF-PAES60 membrane were estimated using the following equation.

$$\Delta V\ (\%) = \frac{V_{mem}^{s} - V_{mem}^{d}}{V_{mem}^{d}} \quad (3)$$

Where V_{mem}^{s} is the membrane volume of the soaked in deionized water at given temperature for 24 h. and V_{mem}^{d} is the membrane volume after the vacuum dried step, respectively.

The mechanical properties were measured using a universal testing machine (Lloyd LR-10K) under ambient conditions (23 ^{o}C under a 45% relative humidity) at a crosshead speed of 10mm min^{-1}. The Dumbbell specimens were prepared using the ASTM standard D638 (type V specimens dog-bone shaped samples). For each measurement, at least five samples were used and their average value was calculated.

Proton conductivity (σ) was calculated using $\sigma = d/RS$, where d is the distance between the reference and sensing electrodes, and S is the cross–sectional area (thickness × width) of the membrane. Measurements at 120 ^{o}C under different humidity conditions were taken as the cell then were equilibriated after relative humidity (RH) cycling. The RH in the cell was achieved by feeding with hydrogen gas, humidified by passing the gas flow through a humidification column. The temperatures of the cell and humidification column were controlled to ensure the desired RH. The BekkTech Test Protocol was applied for conductivity tests. The measurements were carried out at 120 ^{o}C of H_2 at 100 kPa under an input flow rate of 500 sccm. A sample was conditioned at 120 ^{o}C and 70% RH for 3 h, and then the conductivity measurements were performed. At each next RH, stabilization time was about 15 min.

TGA analyses were carried out under air using a TA Instrument Q5000IR at temperatures from 30 to 400 ^{o}C with a heating rate of 10 ^{o}C min^{-1}. Before the TGA measurement, the samples were soaked in Deionized water at 30 ^{o}C for 24 h. After which the samples were removed from the water, wiped off the excess surface water and equilibrated at 30 ^{o}C, 40% RH for 3 h [27].

Result and discussion

[3.1.1 Synthesis of sulfonated PAES60 and preparation of pristine PAES60 membrane]

Sulfonated PAES60 was synthesized via K_2CO_3 catalyzed nucleophillic aromatic substitution polymerization of DCDPS and SDCDPS with DHBP, as indicated in scheme 1. NMP was used as the solvent with toluene as the azeotropic dehydrating agent. PAES60 was chosen as a typical filling material of the pore-filling membrane and fabricated as a pristine membrane to compare with the PF-PAES60 membrane. Figure 1 shows the result of ^{1}H-NMR measurement of the PAES60. Degree of sulfonation calculated from ^{1}H-NMR data [29] was similar to the feed molar ratio of SDCDPS monomer. The experimental IEC value derived from titration test was also close to the theoretical values obtained from ^{1}H-NMR spectra (Table 1). From these measurements and additional results of GPC measurement, the PAES60 polymer with high molecular weight was synthesized successfully.

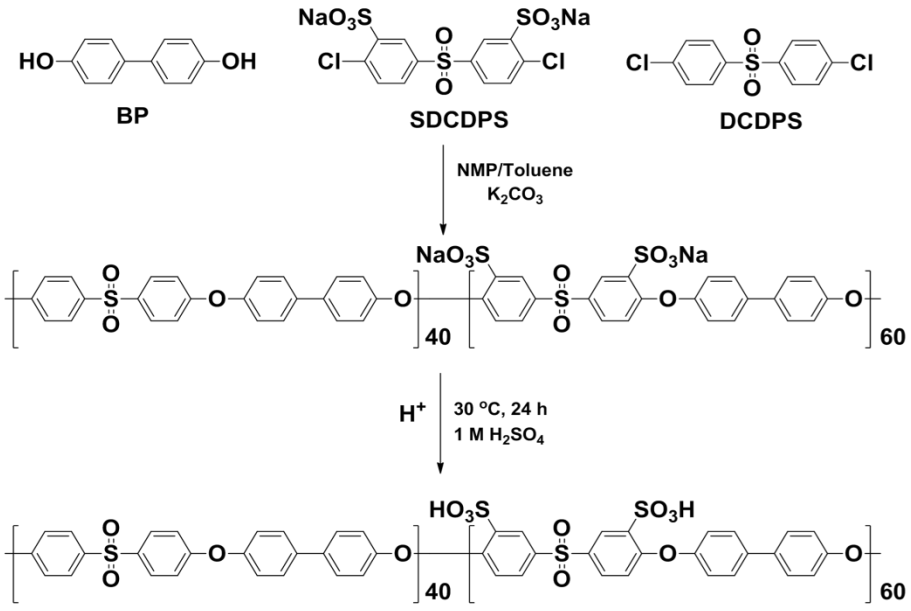

Scheme 1. Synthesis of sulfonated PAES60 copolymer.

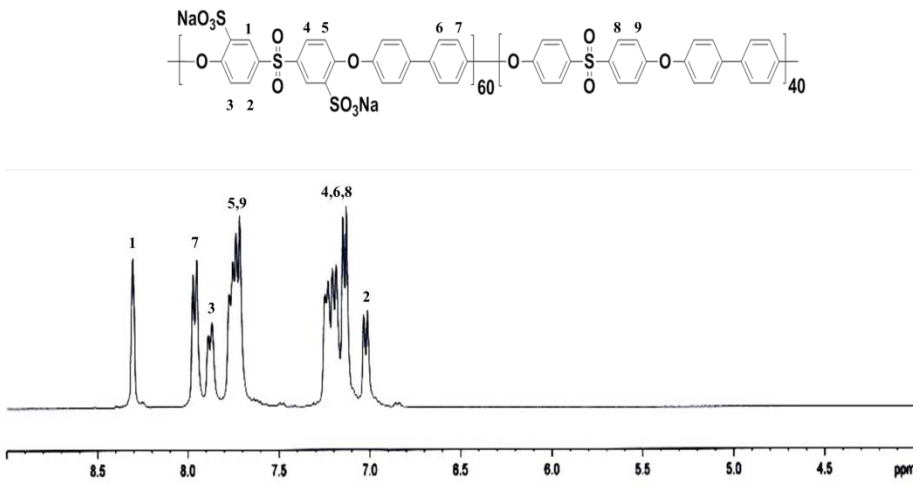

Figure 1. ^{1}H-NMR spectrum of PAES60 in DMSO-*d*.

Polymer	Sulfonation Degree x (%)		IEC_w (mequiv./g)		Mw	Mn	Mw/Mn
	Monomer[a]	^{1}H-NMR[b]	Calcd.	Expt.[c]			
PAES60	60	57	2.13	2.10	106,400	43,100	2.46

[a] Sulfonated degree obtained from monomer ratio.
[b] Sulfonated degree obtained from ^{1}H NMR data.
[c] Determined experimentally by acid-base titration.

Table 1. Properties of PAES60.

[3.1.2 Preparation of porous P(*p*Bu-co-BI) substrates and pore-filling (PF-PAES60) membrane]

Porous P(*p*Bu-co-BI) substrates were prepared by leaching out a DBP form P(*p*Bu-co-BI)/DBP films. By this method, illustrated in Scheme 2, DBP which is a kind of plasticizer-type compound was used as a template for making pore into P(*p*Bu-co-BI) films. In the first stage, P(*p*Bu-co-BI)/DBP films were prepared by casting P(*p*Bu-co-BI)/DBP mixtures. During the film formation, once the solvent is evaporated, phase separation occurs, leading to a P(*p*Bu-co-BI)/DBP blend. In the second stage, the DBP is leached out from the films by immersion in methanol, which is a selective solvent for the DBP, leading to a porous film. Thus, the morphology of the porous films is related to the P(*p*Bu-co-BI)/Porogen blend composition.

PF-PAES60 membrane fabricated by polymer dipping method illustrated in Scheme 2. To facilitate the subsequent polymer infiltration, PAES60 was dissolved in a DMF to decrease the viscosity. And filling temperature is increased at 60 ^{o}C for making the slightly expended state of the porous P(*p*Bu-co-BI) film. During the filling step of the PAES60 polymer into the pores of the porous substrate, the gravity force dragged PAES60 solution into the pores of the porous P(*p*Bu-co-BI)

substrate. Then, the PAES60 macromolecules grow along the pores of the P(*p*Bu-co-BI) substrate when the solvents were completely evaporated [30].

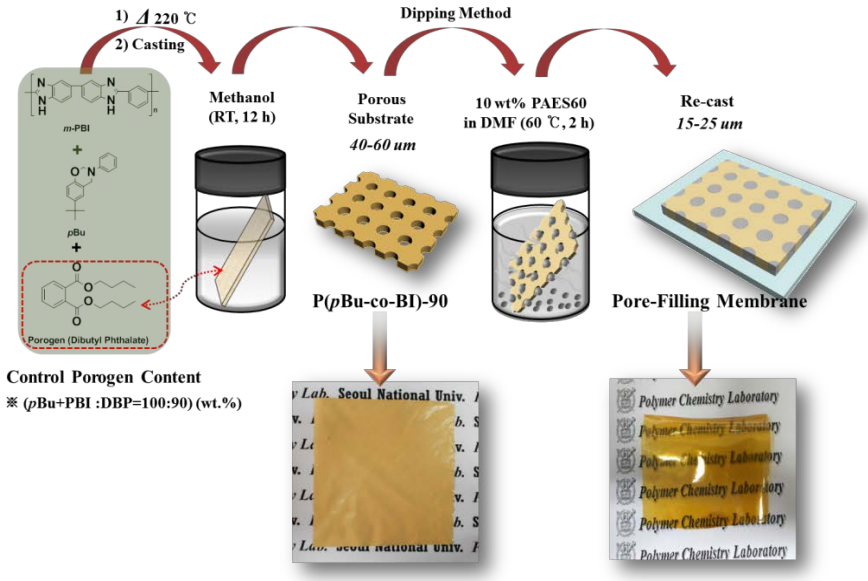

Scheme 2. Preparation process of PF-PAES60 membrane.

[3.2.1 Morphological analysis and SEM, EDS measurements of the membranes]

Changing the porogen content to *p*Bu and PBI weight percent, Pore-size and porosity of the porous P(*p*Bu-co-BI) substrate were calculated from the mercury intrusion method and density measurement method. Table 2 shows the pore-size and porosity results generated with DBP in 50, 70, 80, 90 wt. % content, respectively. When the porogen content was increased over the 90 wt. % of *p*Bu and PBI, the membranes were too brittle and separated. Therefore, the maximum content of the DBP was 90% of the *p*Bu and PBI weight. From the mercury instrument measurement results, when the DBP content increased, membranes experienced an increase in pore-size while the porosity was not changed. However, another porosity results, obtained from the density measurement and eq. (1), showed that the content of the DBP affect the porosity of the membranes. Moreover, porosity obtained from density measurement method was smaller than that of the mercury intrusion method. Previous report suggests that investigated methods of the calculating the porosity are complementary and each method is robust to characterize specific aspect of the porous materials [31]. Because each method applied different principles and different approaches.

Considering the limitation of each method, they can provide reliable data on a given aspect of porosity. So all of the pore-size and porosity results calculated from two types of method were accepted the valid results.

From the Table 2, we selected the P(*p*Bu-co-BI)-90 as a porous substrate in this experiment because it has not only large pore-size and high porosity which is affecting the proton conductivity of the membrane owing to the large amount of PAES60 polymers can filled inside of the porous substrate but also high mechanical strength sufficient to use the reinforcement of the pore-filling membrane.

SEM was additionally employed to investigate the pore-size of the porous P(*p*Bu-co-BI)-90 substrate. Figure 2 shows the cross-sectional image of the P(*p*Bu-co-BI)-90 substrate. SEM image shows that some pores very large in diameter (1-2 um) contributed to interior structure of porous substrates. Putting pore-size results obtained from mercury intrusion method and SEM image together, porous P(*p*Bu-co-BI)-90 substrate has the macro pores varies from <100 nm of the interconnected channel size (detected by mercury intrusion) to 1-2 um with spherical shape of cross-sectional pores (detected by SEM).

Figure 3. Shows the SEM images of the PF-PAES60 membrane cross-section and EDS mapping for the carbon, nitrogen, sodium elements.

From the SEM image (see micrograph of Fig. 3.), the thickness of the PF-PAES60 membrane was 22um.

To qualitatively characterize PF-PAES60 membrane structure, the EDS mappings of the elements for determining the elemental distribution along the membrane cross-section were employed. In the display, light areas corresponded to a high content of the elements. The carbon element is wholly distributed along the cross-section of the PF-PAES60 membrane for its presence in both the P(*p*Bu-co-BI) and PAES60 components. Also, the nitrogen element is almost distributed along the membrane cross-section owing to the presence of P(*p*Bu-co-BI), and its concentration seemed to be less than that of the carbon element due to the existence of the nitrogen-free PAES60. However, it was still an important concern that whether the hydrophilic PAES60 was properly impregnated into the hydrophobic P(*p*Bu-co-BI). The unique sulfonic acid group (-SO3H) of the PAES60 ionomer could be a choice to determine the distribution of the PAES60 component in the PF-PAES60 membrane. However, to analyze the elemental content in the PF-PAES60 membranes, the two types of sulfur element should be distinguished. For easy description of the sulfonic group, the sodium ion (Na) was a good tracer-candidate for the EDS measurement. The signal Na element for marking of the PAES60 component also

displayed a homogeneous distribution in the membrane cross-section. Therefore, the distribution of the sulfur and sodium elements along the cross-sectional PF-PAES60 membrane suggested that the PAES60 ionomer component might be homogeneously impregnated in the P(*p*Bu-co-BI)-90 substrate.

	Porogen content (wt. %)					
	0	50	70	80	90	120
Average Pore Diameter (4V/A) (Å)	(-)	307	421	463	513	631
Porosity (Vol.%) – Mercury Intrusion	(-)	63.6	65.7	66.3	65.6	65.9
Density (g/cm^3)	1.11	0.63	0.58	0.55	0.51	0.42
Porosity (Vol.%) – Density Measurement	(-)	48.1	52.0	55.4	58.6	63.1

Table 2. Structural properties of P(*p*Bu-co-BI)-X substrates prepared by changing the porogen content (wt. %).

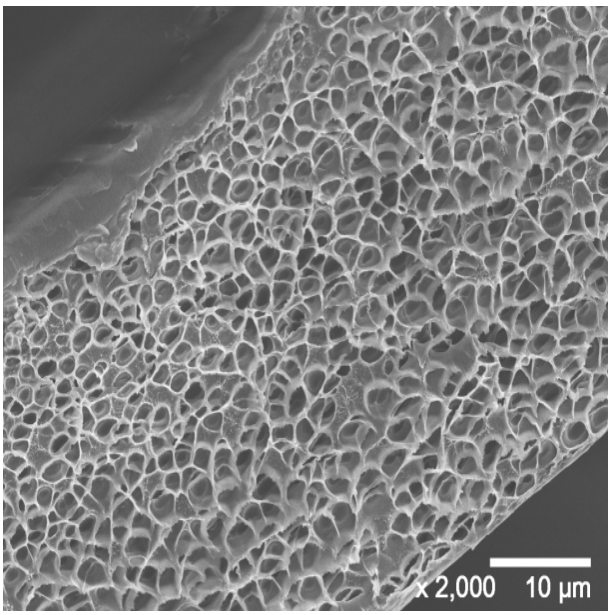

Figure 2. SEM image of the cross-sectional porous P(*p*Bu-co-BI)-90 substrate.

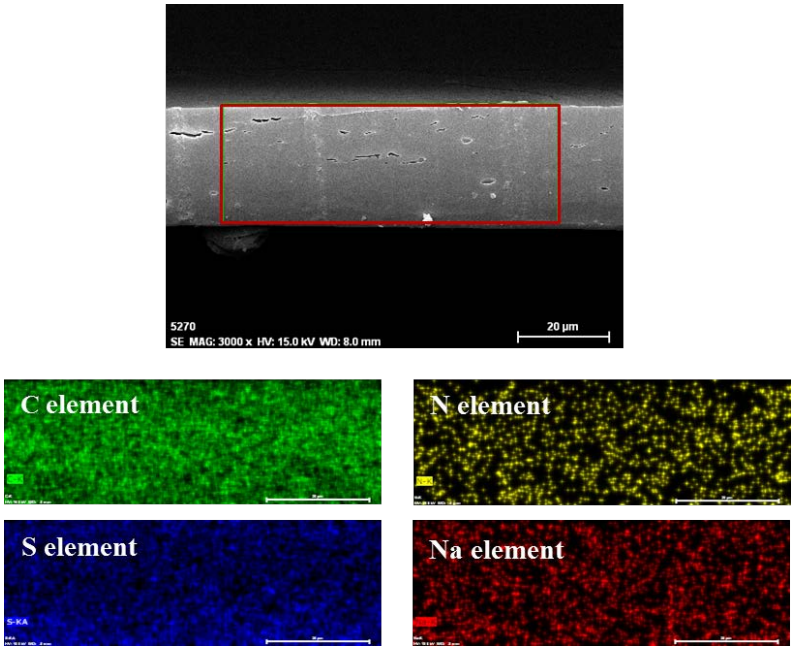

Figure 3. SEM image of the cross-sectional PF-PAES60 membrane and EDS mappings for the carbon, fluorine, sulfur and sodium elements.

[3.2.2 Characterization of PAES60 and PF-PAES60 Membranes]

[FT-IR spectroscopy]

Figure 4. shows the FT-IR spectra analysis of the porous substrate (P(*p*Bu-co-BI)-90), pristine PAES60 membrane (60H, 60Na) and PF-PAES60 membrane (PF-60H, PF-60Na). When the membranes underwent protonation step or not, the name of samples were represented by 60H and 60Na, respectively. Compared with the IR bands corresponding to the sulfur moieties of the 60H and PF-60H, existence of the interaction between the P(*p*Bu-co-BI)-90 and 60H was confirmed. Symmetric, asymmetric stretching of $-SO_3^-$ and the symmetric stretching band of the sulfone ($-SO_2-$) in the 60H were observed at 1024 cm^{-1}, 1095 cm^{-1} and 1146 cm^{-1}, respectively [32]. In the case of PF-60H, the symmetric and asymmetric stretching of $-SO_3^-$ of the PF-60H membrane shifted to 1024 cm^{-1} and 1095 cm^{-1}, respectively. however, the symmetric stretching band of the sulfone ($-SO_2-$) which lies at 1146 cm^{-1} remains insensitively. This result indicates that the P(*p*Bu-co-BI)-90, especially, imidazole groups in the P(*p*Bu-co-BI)-90 structure interacted with the sulfuric acid groups in

the 60H polymer as opposed to some other functional unit in the backbone [33, 34]. To further confirm the acid-base interaction with P(*p*Bu-co-BI)-90 and PAES60, 60Na and PF-60Na were also measured. The peak positions corresponding to the -SO_3^- are detected at same wavenumbers in both case of 60Na and PF-60Na.

From these results, the acid-base interaction of the porous P(*p*Bu-co-BI)-90 substrate and PAES60 was elucidated.

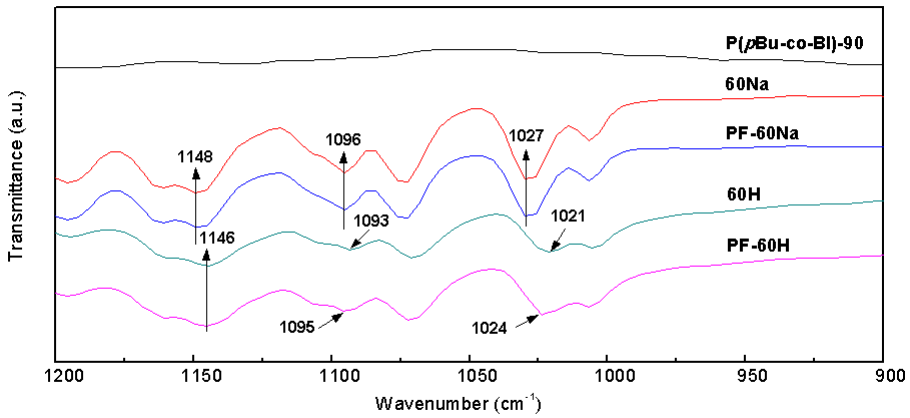

Figure 4. FT-IR spectral analysis of the the porous P(*p*Bu-co-BI)-90 substrate, pristine PAES60 membrane (60Na, 60H) and PF-PAES60 membrane (PF-60Na, PF-60H).

[Swelling properties]

The water content of the polymer electrolyte membrane is important factor affecting the proton conductivity and transport phenomena. [29] Excess swelling of the electrolyte membrane leads to low mechanical durability and dimensional change, which could be a reason for low fuel cell performances when fabricated into a membrane electrode assembly (MEA) [35]. Figure 5 (a) Shows a comparison of the PAES60 membrane and PF-PAES60 membrane after being soaked in deionized water at given temperature for 24 h. PAES60 displayed a much exaggerated water uptake at 100 ^{o}C, so its value could not be obtained. PAES60 membrane showed a rapidly increased water uptake at over 40 ^{o}C owing to existence of the percolation limit of high sulfonation degree of PAES [21]. However, the water uptake of the PF-PAES60 membrane was quite low (10-18%), even at elevated temperature.

The dimensional change (Figure 5 (b)) of the membranes displayed the similar trend. At 100 ^{o}C, The PAES60 membrane was not sustained its volume because of high water uptake. Also swelling of the PAES60 membrane increased rapidly at over 40 ^{o}C. However, at all the given temperature range, the dimensional change of PF-PAES60 membrane was in the range of 4-13%. From the results (Figure 5 (a), (b)), PF-

PAES60 membrane exhibited a much lower water uptake and dimensional change. These results were attributed to the existence of the base-type porous P(*p*Bu-co-BI)-90 substrate. The rigid porous P(*p*Bu-co-BI)-90 substrate can effectively suppress the membrane from swelling and prevent the membrane from absorbing excess water. Furthermore, the basic imidazole unit in the P(*p*Bu-co-BI)-90 structure also contributed to the increasing stability of the pore-filling membrane, owing to the effect of ionic cross-linking resulted from the acid-base interaction between imidazole groups and sulfonic acid groups in the PAES60. Therefore, PF-PAES60 membrane maintained excellent physical stability after soaked in boiling water for 24 h. This result suggests that PF-PAES60 membrane has a good potential for high temperature fuel cell applications.

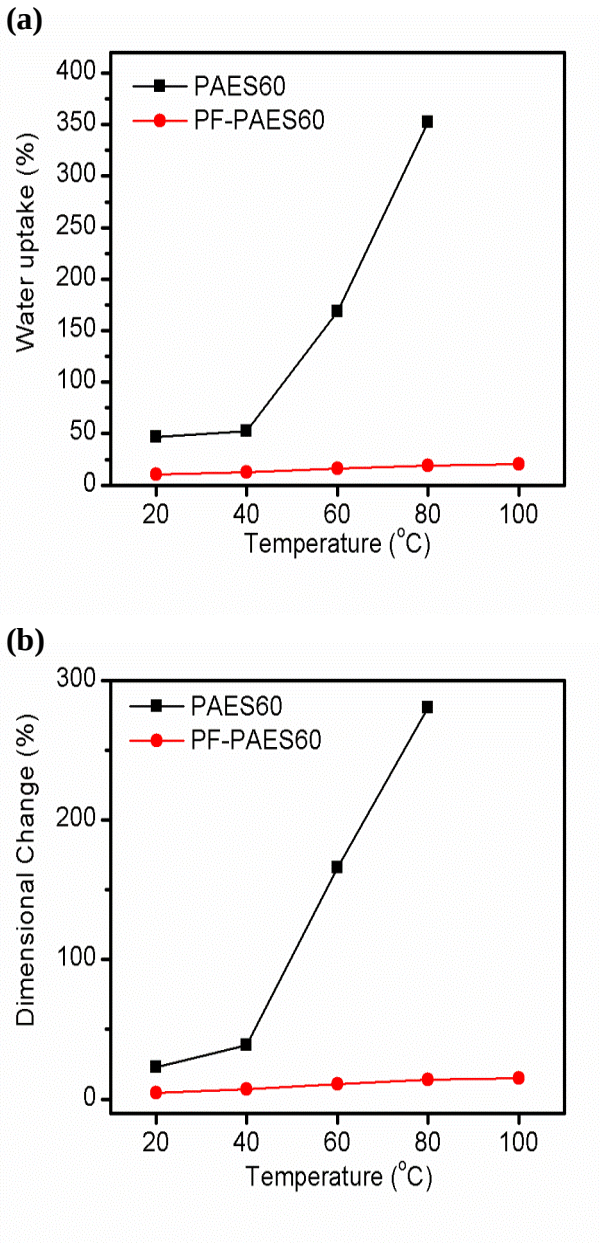

Figure 5. Comparison of swelling properties for pristine PAES60 membrane and PF-PAES60 membrane: (a) water uptake; (b) Dimensional change.

[Mechanical Strength]

Figure 6. shows a comparison of the mechanical properties of the pristine PAES60 and PF-PAES60 membranes. The name of the samples is same with the explained in FT-IR spectroscopy section. PF-60H membrane showed outstanding mechanical strength, e.g. young's modulus (Figure 6 (a)) and tensile strength (Figure 6 (b)) than that of 60H membrane because of the reinforcement effect of the P(*p*Bu-co-BI)-90 substrate. But the elongation at break (Figure 6 (c)) of the PF-60H membrane was decreased than that of 60H membrane because rigid polymer structure and hydrophobicity of the P(*p*Bu-co-BI) substrate hindered the chain mobility and water uptake of the PF-60H. To confirm the contribution of the acid-base interaction to the mechanical properties of the Pore-filling membrane, 60Na and PF-60Na were measured, additionally. Comparing with 60H and 60Na membranes, 60Na shows better mechanical toughness than 60H membrane. Because sodium sulfate group of the 60Na membrane was existed in the salt state, so it can increase the membrane's stiffness. However, in the case of the PF-60H membrane, this membrane showed better mechanical toughness than that of PF-60Na, resulted from the additional ionic cross-linking induced from the acid-base interaction

between imidazole group in the P(*p*Bu-co-BI)-90 substrate and sulfuric acid group in the 60H polymer [36]. From the mechanical properties data, PF-60H membrane showed outstanding mechanical toughness because of the not only reinforcement effect of the P(*p*Bu-co-BI)-90 substrate, but also additional ionic cross-linking effect generated from the acid-base interaction. Higher mechanical strength allows fabrication of thinner membranes with smaller resistance. So it can affect the operating condition and durability of the MEA. Therefore, PF-60H membrane suggests a good potential for high temperature fuel cell applications [37].

(a)

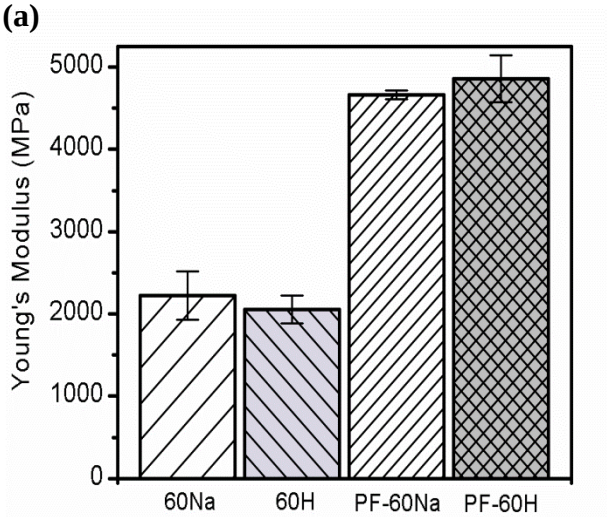
Young's Modulus (MPa)
5000
4000
3000
2000
1000
0
60Na
60H
PF-60Na
PF-60H

(b)

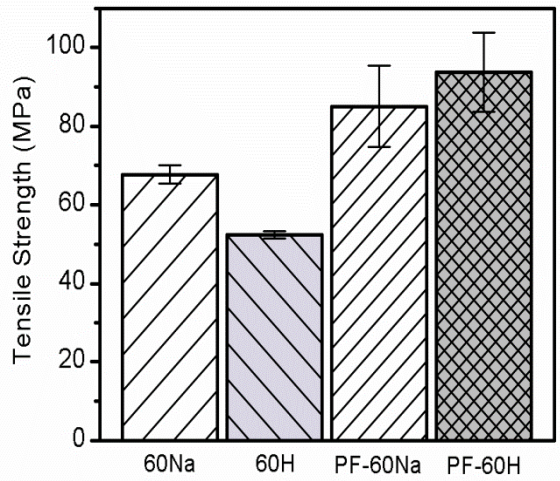
Tensile Strength (MPa)
100
80
60
40
20
0
60Na
60H
PF-60Na
PF-60H

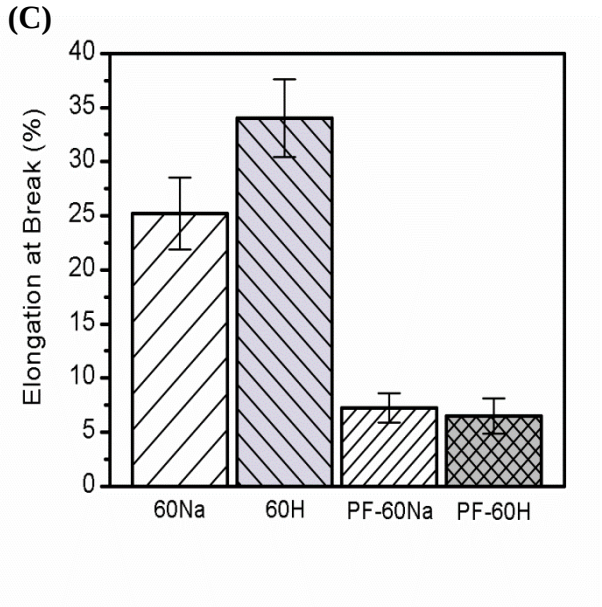

Figure 6. Comparison of mechanical properties of pristine PAES60 membranes (60Na, 60H) and PF-PAES60 (PF-60Na, PF-60H) membranes: (a) Young's modulus; (b) Tensile strength (C) Elongation at break.

[Proton Conductivity]

The proton conductivity of the PF-60H membrane was examined and compared with that of the 60H membrane. Figure 7. exhibited that the relative humidity (RH) dependent proton conductivities of both membranes increased as the measurement humidity was increased from 19.6 to 96 % at 120 ^{o}C. Meanwhile, over a wide range of RH, the PF-60H membrane showed lower proton conductivity than the 60H membrane. This phenomena in the proton conductivity was ascribed to the existence of the P(*p*Bu-co-BI)-90 substrate. In general, the proton conductivity of pore-filling membranes is heavily dependent on the porosity and porous structure of substrates, because proton transport takes place exclusively in the pore-impregnating electrolytes. The porosity of the P(*p*Bu-co-BI)-90 substrate measured from mercury intrusion method was 65 %, which reveals the existence of inactive volume for proton transport in the PF-60H membrane, consequently leading to the reduction in the proton conductivity. Another effect of reduced proton conductivity is the interaction between the imidazole group and the sulfonic acid group. Acid-base interaction decreased the acidity and proton mobility of the membrane.

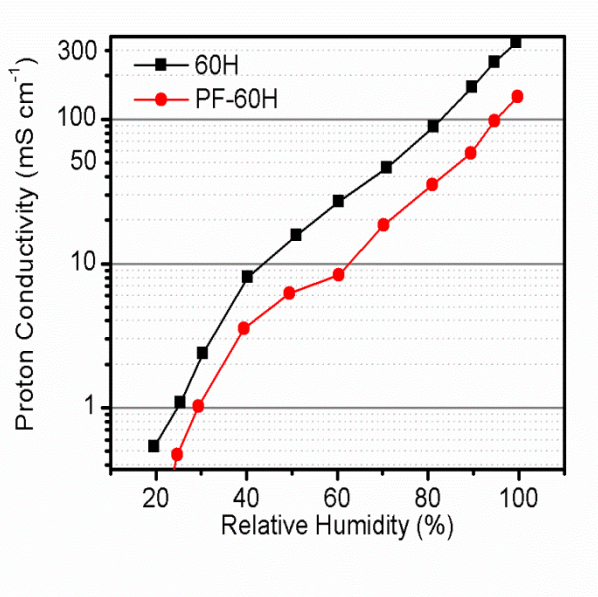

Figure 7. Relative-humidity dependent proton conductivity of pristine PAES60 membrane and PF-PAES60 membrane at 120 ^{o}C.

[TGA Analysis]

In an effort to understand the proton conductivity of the membranes at the harsh operating condition, the state of water in the membranes was investigated. Previous reports [38-40] described that the state of water in water-swollen membranes could be classified into two types based on the analysis of TGA data: physically bounded water (i.e. slightly bound water) and chemically bounded water (i.e. strongly bound water). More specifically, the weight loss below 100 ^{o}C can be attributed to the vaporization of physically bounded water in the membranes and the weight loss between 100 ^{o}C and 300 ^{o}C (total water content in membranes - the weight below 100 ^{o}C) can be ascribed to the vaporization of chemically adsorbed water via hydrogen bonding and desorption of hydroxyl group. However, other report [41] was concerned that the quantitative use of thermodynamic data to prove the state of water in the water-swollen membranes. Thus, in this study; the characterization of water state based on the TGA data has been restricted to a relative comparison between the samples, rather than elucidate the absolute value of the state of water. Figure 9 (a). showed that the total water contents of the PAES60 and PF-PAES60 membranes were observed to 11.5 wt. % and 8.5 wt. %

respectively. More specifically, for the PAES60 membrane, the physically observed water is 80.8% and the weight loss attributed to the chemically adsorbed water is 19.2%. In comparison, for the PF-PAES60 membrane, the weight loss of the physically adsorbed water was 32.6% and the weight loss of the chemically adsorbed water was 67.4%. The relatively fraction of physically adsorbed and chemically adsorbed water in the total water content are summarized in Figure 9 (b). The fraction of chemically absorbed water in the PF-PAES60 membrane was higher than that in the PAES60 membrane. These TGA results indicate that the PF-PAES60 membrane can hold a larger amount of chemically adsorbed water owing to the existence of P(*p*Bu-co-BI)-90 substrate and the effectiveness of the acid-base interaction with the base type porous substrate and acidified filling material.

Physically adsorbed water is known to act as a proton-transfer medium that follows the vehicle mechanism, while chemically adsorbed water is involved in the Grotthus mechanism by forming hydrogen bonds [42]. In dehumidified conditions, proton conduction is predominantly governed by Grotthus mechanism rather than the vehicle mechanism. Under these harsh operating conditions the contribution of chemically adsorbed water becomes more pronounced. Accordingly,

the increase in the chemically adsorbed water of the PF-PAES60 membrane could reasonably explain the similar proton conductivity value of the PAES60 membrane. From the water state obtained by TGA analysis can be support to explain facilitate proton conduction of pore-filling membranes at high temperature and low humidity condition.

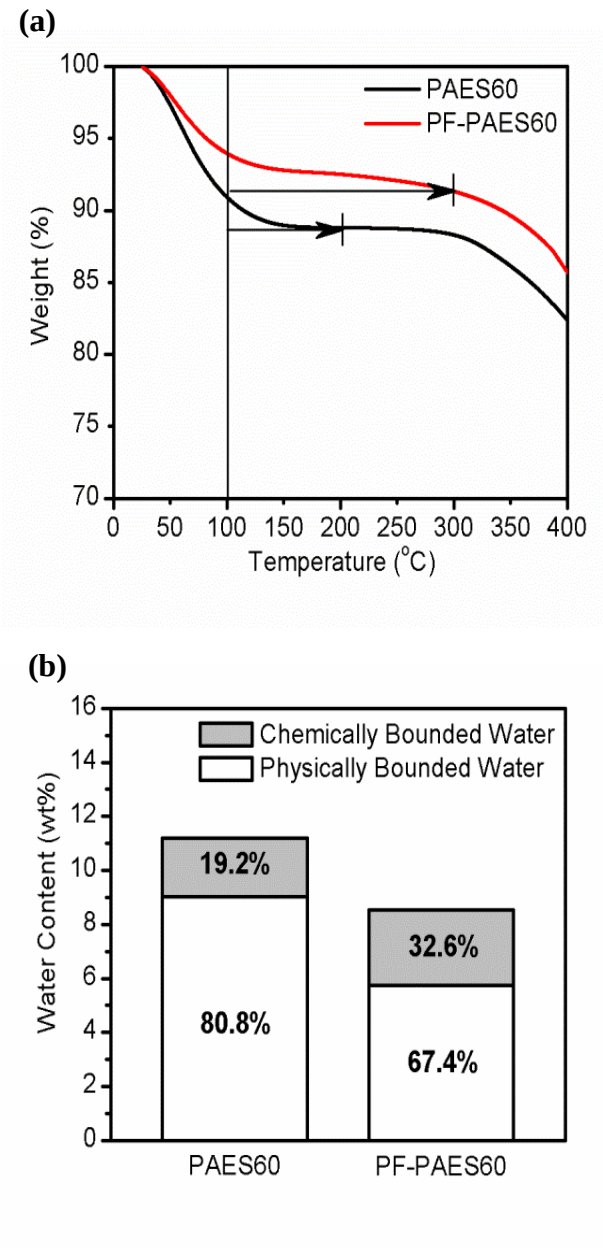

Figure 8. Analysis of state of water for pristine PAES60 membrane and PF-PAES60 membrane: (a) TGA thermograms (b) relative fractions of physically adsorbed water and chemically adsorbed water in total water content of membranes.

4. Conclusion

The reinforced pore-filling type polyelectrolyte membrane was prepared using porous P(*p*Bu-co-BI)-90 substrate with sulfonate PAES60 polymer. Porous P(*p*Bu-co-BI)-90 substrate was successfully fabricated by leaching out a porogen (DBP) compound using a selective solvent of the DBP from P(pBu-co-BI) / DBP mixtures. The PF-PAES60 membrane showed excellent properties compared to PAES60 membrane. Such as lower dimensional change and water uptake even at elevated temperature, higher mechanical strength, and higher chemically bounded water content in low humidity condition. The improved performance of the PEMFC with PF-PAES60 membrane was also demonstrated, as evidenced by a 20% higher OCV value and much more increased retention time of OCV at 120 ℃, 40% humidity conditions than PAES60 membrane. The PF-PAES60 membrane is very a good candidate for use in promising as a proton exchange membrane for proton exchange membrane for PEMFC applications.

5. Acknowledgements

This research was supported by Samsung Advanced Institute of Technology, Samsung Electronics Co., Ltd. through the Brain Korea Program and the Fundamental R&D Program of World Premier Materials (WPM) funded by the Ministry of Knowledge Economy, Republic of Korea.

6. References

1. Alberti, G. and M. Casciola, *Composite membranes for medium-temperature PEM fuel cells.* Annual Review of Materials Research, 2003. 33: p. 129-154.
2. Higashihara, T., K. Matsumoto, and M. Ueda, *Sulfonated aromatic hydrocarbon polymers as proton exchange membranes for fuel cells.* Polymer, 2009. 50(23): p. 5341-5357.
3. Nakabayashi, K., T. Higashihara, and M. Ueda, *Polymer Electrolyte Membranes Based on Cross-Linked Highly Sulfonated Multiblock Copoly(ether sulfone)s.* Macromolecules, 2010. 43(13): p. 5756-5761.
4. Li, Q., et al., *Cross-Linked Polybenzimidazole Membranes for Fuel Cells.* Chemistry of Materials, 2007. 19(3): p. 350-352.
5. Asensio, J.A., S. Borrós, and P. Gómez-Romero, *Proton-conducting polymers based on benzimidazoles and sulfonated benzimidazoles.* Journal of Polymer Science Part A: Polymer Chemistry, 2002. 40(21): p. 3703-3710.
6. Lee, H.-S., et al., *Synthesis and characterization of poly(arylene ether sulfone)-b-polybenzimidazole copolymers for high temperature low humidity proton exchange membrane fuel cells.* Polymer, 2008. 49(25): p. 5387-5396.
7. Wang, C., et al., *Composite Membranes with Sulfonic and Phosphonic Functionalized Inorganics for Reduced Relative Humidity PEM* Fuel *Cells.* Journal of The Electrochemical Society, 2011. 158(6): p. B690-B697.
8. Lakshminarayana, G., et al., *Anhydrous Proton Conducting Hybrid Membrane Electrolytes for High Temperature (>100°C) Proton Exchange Membrane Fuel Cells.* Journal of The Electrochemical

Society, 2011. 158(4): p. B376-B383.

9. Choi, B.G., et al., *Innovative Polymer Nanocomposite Electrolytes: Nanoscale Manipulation of Ion Channels by Functionalized Graphenes.* Acs Nano, 2011. 5(6): p. 5167-5174.
10. Tseng, C.Y., et al., *Sulfonated Polyimide Proton Exchange Membranes with Graphene Oxide show Improved Proton Conductivity, Methanol Crossover Impedance, and Mechanical Properties.* Advanced Energy Materials, 2011. 1(6): p. 1220-1224.
11. Liu, F., et al., *Nafion/PTFE composite membranes for fuel cell applications.* Journal of Membrane Science, 2003. 212(1–2): p. 213-223.
12. Zhang, Y., et al., *Fabrication and characterization of a PTFE-reinforced integral composite membrane for self-humidifying PEMFC.* Journal of Power Sources, 2007. 165(2): p. 786-792.
13. Kim, K.-H., et al., *Characteristics of the Nafion®-impregnated polycarbonate composite membranes for PEMFCs.* Electrochimica Acta, 2004. 50(2–3): p. 577-581.
14. Alwin, S., et al., *Modified-Pore-Filled-PVDF-Membrane Electrolytes for Direct Methanol Fuel Cells.* Journal of The Electrochemical Society, 2011. 158(2): p. B91-B98.
15. Nguyen, T.H., C. Wang, and X. Wang, *Pore-filling membrane for direct methanol fuel cells based on sulfonated poly(styrene-ran-ethylene) and porous polyimide matrix.* Journal of Membrane Science, 2009. 342(1-2): p. 208-214.
16. Kim, S.K., et al., *Cross-Linked Benzoxazine-Benzimidazole Copolymer Electrolyte Membranes for Fuel Cells at Elevated Temperature.* Macromolecules, 2012. 45(3): p. 1438-1446.
17. Kim, S.K., et al., *Durable cross-linked copolymer membranes based on poly(benzoxazine) and poly(2,5-benzimidazole) for use in fuel cells at elevated temperatures.* Journal of Materials Chemistry, 2012. 22(15): p. 7194-7205.

18. Mecerreyes, D., et al., *Porous Polybenzimidazole Membranes Doped with Phosphoric Acid: Highly Proton-Conducting Solid Electrolytes.* Chemistry of Materials, 2004. 16(4): p. 604-607.
19. Jouanneau, J., et al., *Synthesis of sulfonated polybenzimidazoles from functionalized monomers: Preparation of ionic conducting membranes.* Macromolecules, 2007. 40(4): p. 983-990.
20. Qi, Y.H., et al., *Synthesis and Properties of Novel Benzimidazole-Containing Sulfonated Polyethersulfones for Fuel Cell Applications.* Journal of Polymer Science Part a-Polymer Chemistry, 2009. 47(7): p. 1920-1929.
21. Wang, F., et al., *Direct polymerization of sulfonated poly(arylene ether sulfone) random (statistical) copolymers: candidates for new proton exchange membranes.* Journal of Membrane Science, 2002. 197(1–2): p. 231-242.
22. Ueda, M., et al., *Synthesis and Characterization of Aromatic Poly(Ether Sulfone)S Containing Pendant Sodium-Sulfonate Groups.* Journal of Polymer Science Part a-Polymer Chemistry, 1993. 31(4): p. 853-858.
23. Wiles, K.B., et al., *Directly copolymerized partially fluorinated disulfonated poly(arylene ether sulfone) random copolymers for PEM fuel cell systems: Synthesis, fabrication and characterization of membranes and membrane–electrode assemblies for fuel cell applications.* Journal of Membrane Science, 2007. 294(1–2): p. 22-29.
24. Schulze, M., et al., *Characterization of polymers in PEFC-electrodes with EDX and XPS.* Fresenius Journal of Analytical Chemistry, 1999. 365(1-3): p. 123-132.
25. Yamaguchi, T., F. Miyata, and S.-i. Nakao, *Pore-filling type polymer electrolyte membranes for a direct methanol fuel cell.* Journal of Membrane Science, 2003. 214(2): p. 283-292.
26. Munakata, H., D. Yamamoto, and K. Kanamura, *Properties of composite proton-conducting membranes prepared from three-*

dimensionally ordered macroporous polyimide matrix and polyelectrolyte. Chemical Communications, 2005(31): p. 3986-3988.

27. Seol, J.-H., et al., *SiO2 nanoparticles-coated poly(paraphenylene terephthalamide) nonwovens as reinforcing porous substrates for proton-conducting, sulfonated poly(arylene ether sulfone)-impregnated composite membranes.* Solid State Ionics, 2011. 190(1): p. 30-37.
28. Li, Y.X., et al., *Synthesis and characterization of controlled molecular weight disulfonated poly(arylene ether sulfone) copolymers and their applications to proton exchange membranes.* Polymer, 2006. 47(11): p. 4210-4217.
29. Hara, N., et al., *Rapid Proton Conduction through Unfreezable and Bound Water in a Wholly Aromatic Pore-Filling Electrolyte Membrane.* Journal of Physical Chemistry B, 2009. 113(14): p. 4656-4663.
30. Zhu, X.B., et al., *Challenging reinforced composite polymer electrolyte membranes based on disulfonated poly(arylene ether sulfone)-impregnated expanded PTFE for fuel cell applications.* Journal of Materials Chemistry, 2007. 17(4): p. 386-397.
31. Fashandi, H. and M. Karimi, *Characterization of porosity of polystyrene fibers electrospun at humid atmosphere.* Thermochimica Acta, 2011. 547: p. 38-46.
32. Kim, Y.S., et al., *Fabrication and characterization of heteropolyacid (H3PW12O40)/directly polymerized sulfonated poly(arylene ether sulfone) copolymer composite membranes for higher temperature fuel cell applications.* Journal of Membrane Science, 2003. 212(1-2): p. 263-282.
33. Jones, D.J. and J. Rozière, *Recent advances in the functionalisation of polybenzimidazole and polyetherketone for fuel cell applications.* Journal of Membrane Science, 2001. 185(1): p. 41-58.
34. Lee, J.K. and J. Kerres, *Synthesis and characterization of sulfonated*

poly(arylene thioether)s and their blends with polybenzimidazole for proton exchange membranes. Journal of Membrane Science, 2007. 294(1–2): p. 75-83.

35. Nguyen, T. and X. Wang, *Multifunctional composite membrane based on a highly porous polyimide matrix for direct methanol fuel cells.* Journal of Power Sources, 2010. 195(4): p. 1024-1030.
36. Wang, J.L., et al., *Highly compatible acid-base blend membranes based on sulfonated poly(ether ether ketone) and poly(ether ether ketone-alt-benzimidazole) for fuel cells application.* Journal of Membrane Science, 2012. 415: p. 644-653.
37. Yamaguchi, T., et al., *An extremely low methanol crossover and highly durable aromatic pore-filling electrolyte membrane for direct methanol fuel cells.* Advanced Materials, 2007. 19(4): p. 592-+.
38. Kim, S.J., C.K. Lee, and S.I. Kim, *Characterization of the water state of hyaluronic acid and poly(vinyl alcohol) interpenetrating polymer networks.* Journal of Applied Polymer Science, 2004. 92(3): p. 1467-1472.
39. Tung, S.-P. and B.-J. Hwang, *High proton conductive glass electrolyte synthesized by an accelerated sol–gel process with water/vapor management.* Journal of Membrane Science, 2004. 241(2): p. 315-323.
40. Zhu, X., et al., *An Ultrathin Self-Humidifying Membrane for PEM Fuel Cell Application: Fabrication, Characterization, and Experimental Analysis.* The Journal of Physical Chemistry B, 2006. 110(29): p. 14240-14248.
41. Kalapos, T.L., et al., *Thermal studies of the state of water in proton conducting fuel cell membranes.* Journal of Power Sources, 2007. 172(1): p. 14-19.
42. Hofmann, D.W.M., et al., *Investigation of Water Structure in Nafion Membranes by Infrared Spectroscopy and Molecular Dynamics Simulation.* The Journal of Physical Chemistry B, 2008. 113(3): p. 632-639.

ABSTRACT IN KOREAN

본 연구에서는 고분자 용액 충진 방법을 이용하여 고분자 연료전지 전해질 막에 이용 가능 한 매우 얇으면서도 기계적 물성이 높은 다공 충진 전해질 막을 제조하였고 이를 분석하였다. 사용된 지지체의 경우 폴리(벤즈이미다졸) (PBI) 과 3-페닐-3,4-디하이드로-6-터트-부틸-2H-1,3-벤족사진 (*p*Bu) 과의 가교 구조의 공중합체 (P(*p*Bu-co-BI))를 합성 하였으며 막 캐스팅 후에 다공성을 부여하기 위해 일정 비율로 혼합한 포로젠 물질인 다이부틸프탈레이트 (DBP)를 선택적으로 녹여내는 방법을 이용하여 다공성 지지체를 제조하였다. 다공성 지지체에 충진하여 수소 이온 전달 역할을 담당할 고분자 물질로는 친핵성 치환 반응을 이용한 축합 중합을 통해 폴리 아릴렌 에테르 술폰 60 (PAES60)를 합성하였으며 이를 충진 물질로 사용하였다. 다공성 지지체 (P(*p*Bu-co-BI)) 와 충진물질 (PAES60)을 이용하여 제조한 다공 충진막 (PF-PAES60)의 경우 기존 PAES60 막에 비해 매우 우수한 치수 안정성을 유지하였으며 기계적 물성이 현저하게 증가된 것을 확인 하였다. 또한 고온, 저 가습 조건에서 셀 성능을 좌우하는 화학적으로 결합된 수분의 비율이 PAES60 막에 비해 매우 높다는 것을 열 분석 결과를 통해 확인하였다. 위와 같은 특징들은 가교 구조의 지지체 도입을 통한 강화 효과뿐만 아니라 지지체와 충진 물질간에 발생한 산-염기 상호작용에 의한 추가적인 물성 향상에서 기인되었다는 것을 본 연구를 통해 확인 할 수 있었다.